

Spatio-Temporal Multiscaling of Solar Surface Flows

J. K. Lawrence and A. C. Cadavid
*Department of Physics and Astronomy
California State University, Northridge*

A. Ruzmaikin
*Jet Propulsion Laboratory
California Institute of Technology*

T. E. Berger
*Lockheed Martin Space and Astrophysics Laboratory
(December 2, 2024)*

The Sun provides an excellent natural laboratory for non-linear phenomena. We use motions of magnetic bright points on the solar surface, at the smallest scales yet observed, to study the dynamics of the photospheric plasma. Random walks display multiscaling over two orders of magnitude in time. Spatial structure functions show multiscaling with exponents approximating the Kolmogorov “K41” values. These results are reconciled within a continuous time random walk framework. This suggests that the observed motions are the walks of imperfectly correlated tracers on a turbulent fluid flow in the lanes between granular convection cells.

In the outer 30% of its radius the Sun’s plasma is convectively unstable, and thermonuclear energy from the core is transported by overturning motion to the visible photosphere. The convective motions are most readily seen as the photospheric pattern of bright “granules” of hot, rising gas, surrounded by a network of “intergranular lanes” of cooler, darker, downflowing gas. The horizontal extent of a granular cell is ~ 1000 km with a range of 200 km to 2500 km. Typical lifetimes are 5 - 15 min.

Magnetic flux threading the solar surface is not uniformly distributed. By processes which are not well understood, it is concentrated into discrete kilogauss fibrils of diameter $\lesssim 150$ km. These accumulate in the intergranular lanes and vertices where they disturb the radiative properties of the photosphere and become apparent to observers through spectral line emission. Such magnetic bright points (MBPs) serve as tracers of the evolution of the granular flow field and of motions in the intergranular network.

With Reynolds number $\approx 10^7$ turbulent flows are expected in the intergranular lanes. Numerical simulations of convection near the solar surface [1] indicate that turbulent vortices are formed in the intergranular lanes where the outflows from neighboring granules collide and turn downward. Observationally, spectrograms taken in magnetically and temperature insensitive spectral lines show line broadening in excess of known Doppler contributions, indicating the presence of turbulent flows on the

borders of granules [2]. These observations cannot rule out other types of motion. The unique, high-resolution data set described below provides access to the actual dynamics and reveals some quantitative characteristics.

Here we study subgranular motions at the highest resolution yet achieved [3–5]. The data were taken on October 5, 1995 with the 50 cm Swedish Vacuum Solar Telescope on La Palma, Spain and consist of two cospatial 71 minute time series of 178 digital images taken essentially simultaneously (within 10 ms). The first set of images was taken through a filter passing wavelengths 430.5 ± 0.5 nm located in the G-band emission of the CH radical. The second set of images was made through a wide-band filter passing wavelengths 468.6 ± 5.0 nm emphasizing the background continuum emission. A 21 Mm \times 21 Mm area of enhanced magnetic activity near the center of the solar disk was imaged, containing hundreds of MBPs. Exposure time was 20 ms, and the pixel scale in the digital images was 60 km on the Sun. The images were checked in real time for seeing sharpness, and the best image pair in each 25 s interval was recorded. Both time series were restored to near the telescope diffraction limit (0.2 arcsec) by phase diversity reconstruction [4]. The final resolution is 165 km in the G-band and 180 km in the broad-band channel. The images were further processed to remove instrumental effects and geometric distortion due to atmospheric seeing.

Next, the wideband images were subtracted from their G-band counterparts, removing most of the granulation pattern common to both sets. Finally the images were subjected to a high-pass spatial filter to emphasize small-scale features [6], and a threshold was imposed to identify MBPs. The result is a three dimensional binary (MBP or not) array with two 350 pixel axes corresponding to x and y spatial directions and a third axis of 178 pixels corresponding to the time. The MBPs undergo significant morphological changes on a time scale of 100 s and are continuously merging and splitting as a result of their interaction with the granular flow [7]. A given MBP is tracked by segmentation of its binary object tree from the data cube. The segmentation is implemented using one-dimensional voxel addressing and searching over limited volumes around a given voxel for valid neighbors. After

segmentation the individual tree is split into branches and the motion of each sub-object is measured with respect to a common reference point.

This procedure delivers strings of x and y positions and times, at roughly 24 s intervals, for 1153 individual MBPs. The longest sequence for an individual MBP object contains 177 data points spanning 71 min, the shortest includes 2 points spanning 9 seconds. During approximately 1 hr the MBPs typically cover an rms distance on the order of a granular diameter.

A typical MBP path is illustrated in Fig. 1. Because of the discrete structuring of the magnetic flux, the motions are naturally described in terms of random walks [8] and diffusion [9]. We use the general form:

$$\langle r^q \rangle^{1/q} = D \cdot t^{\gamma(q)/2} \quad (1)$$

where r is the total displacement during time t , and an appropriately weighted average is taken over all observed displacements. Fig. 2 shows $\langle r^q \rangle^{1/q}$ versus t for different q . In each case we see excellent scaling covering two orders of magnitude in time up to about 40 min. Fig. 3 shows $\gamma(q)$ to be a decreasing function of q . Brownian walks give $\gamma(q) = 1$ for $q > -1$.

The subdiffusion ($\gamma(2) < 1$) indicated by the temporal multiscaling analysis can be related to delays between walk steps on all time scales. If the delay times have a probability density function (pdf) with a power law tail $p(t) \sim t^{-1-\alpha}$ with $\alpha \leq 1$ the value of $\gamma(q)$ in Eq. (1) is reduced by a factor α [10]. Such a property appears naturally [11] in a cellular diffusion model [12] based on an evolving field of identical, outflowing, circular cells which produces changing stagnation points. This in turn gives a subdiffusive random walk of the flow markers, with waiting times on a wide range of scales. The $\gamma(q)$ from a numerical simulation of such a model is included in Fig. 3. Although the motion is correctly subdiffusive at $q = 2$, when the analysis includes $q \neq 2$ the simple trapping idea fails. Although diffusion studies are nearly universally limited to mean square displacements, in this case the general q dependence is critical. We will see that $\gamma(0)$ actually is most informative about the nature of the MBP walks.

Additional dynamical information can be obtained from the spatial scaling of the MBP longitudinal velocity correlations. We determine velocities for all of the MBPs appearing in two consecutive images in the time series. Then for all pairs of MBPs which appear in the same two consecutive images we calculate the longitudinal velocity $\Delta v_{||}(\Delta\ell) = |v_{||}(\mathbf{r} + \Delta\ell) - v_{||}(\mathbf{r})|$, where $v_{||} = (\mathbf{v} \cdot \Delta\ell) / \Delta\ell$, and $\Delta\ell = |\Delta\ell|$ is the spatial separation of the pair. The velocity structure functions are

$$\langle \Delta v_{||}^q(\Delta\ell) \rangle \equiv \langle |v_{||}(\mathbf{r} + \Delta\ell) - v_{||}(\mathbf{r})|^q \rangle = |\Delta\ell|^{\zeta(q)}. \quad (2)$$

The average is taken over all MBP pairs in all pairs of consecutive images. Fig. 4 displays $\langle \Delta v_{||}^q \rangle$ vs $\Delta\ell$ for $q = 2, 3$.

The spatial correlations of the MBP motions show multiscaling, as seen in Fig. 4, between ~ 100 km and ~ 1200 km. The exponents of the longitudinal velocity structure functions $\zeta(q)$ shown in Fig. 5 approximate the Kolmogorov [13] ‘‘K41’’ form for Navier-Stokes turbulence: $\zeta_K = q/3$. At higher moments, $q \gtrsim 6$, the values are probably unreliable, but the exponents may turn below the K41 values, a correction typically due to intermittence [14]. We find that $\zeta(2) = 0.68 \pm 0.14 \approx 2/3$ which is equivalent to the K41 spatial power spectrum exponent $-1 - \zeta(2) \approx -5/3$.

Treating the MBPs as particles undergoing random walks leads to temporal multiscaling and apparent subdiffusion. Conversely, the spatial scaling of the velocity structure functions resembles that of K41 turbulence on subgranular scales, pointing to ‘‘Richardson’’ ($\gamma(q) = 3$) superdiffusion [15]. These phenomena can be reconciled naturally within the framework of the continuous time random walk (CTRW) approach [10]. This can incorporate the effects of power law spatial steps due to underlying fluid motion, correlation of the spatial step lengths with elapsed time, intermittent waiting times at accumulation points, and varying degrees of correlation of the tracers with underlying fluid motions. Previous application to the dynamics of passive tracers in a turbulent fluid has revealed in particular that ‘‘Kolmogorov scaling does not necessarily imply Richardson’s law [16]’’.

The CTRW method focuses on the statistical properties of the phenomena. The central concept is the pdf $\psi(r, t)$ of making a step of length r taking a time interval t . From this basic definition it is possible to calculate analytically the mean square displacement or to calculate by numerical simulation the moments of the displacement of arbitrary order q . We use a pdf with the scaling form $\psi(r, t) = Cr^{-(\sigma+d-2+1/\nu)}\delta(r-t^\nu)$, where $d = 2$ is the spatial dimension, $\nu = 3/2$ couples the spatial and temporal steps so as to incorporate K41 spatial correlations, and σ characterizes the pdf of the step lengths and governs the degree of correlation between tracers and fluid flow [16]. This also provides a simple repetitive simulation algorithm: step in a random direction by a distance chosen from a pdf $\propto r^{-\sigma}$ while advancing the time by $t \propto r^{1/\nu}$. We will not include stagnation times.

With our choice of parameters one finds both analytically and numerically [17] that for $\sigma \leq 5/3$, $\gamma(2) = 3$ (Richardson diffusion), for $5/3 < \sigma < 3$, $\gamma(2) = 11/2 - 3\sigma/2$ and for $\sigma \geq 3$, $\gamma(2) = 1$ (Brownian diffusion). In the Richardson case the mean correlation time of the tracers with the flow $\langle \tau \rangle$ is infinite; the tracers fully represent the flow pattern. In the intermediate case $\langle \tau \rangle$ is finite although $\langle \tau^2 \rangle$ is infinite. In the Brownian case $\langle \tau \rangle$ and $\langle \tau^2 \rangle$ are finite. For $2 \leq \sigma \leq 7/2$ we have numerically extended the intermediate and Brownian results to include $\gamma(q)$ with moments $0.2 \leq q \leq 4$. The convergence of the simulation is quite rapid for $q \ll 1$. The solar data give $\gamma(0) \approx 1.3$ selecting the intermediate regime.

In the limit of infinite trials $\gamma(q) \rightarrow const.$ which differs from the decreasing $\gamma(q)$ shown by the solar MBPs.

However, the actual data set is limited in time and the number of tracers, so it is necessary for us to dig more deeply into the statistics. Let $\tilde{\gamma}(q)$ represent the diffusion exponent calculated by averaging over 100 walks, which roughly matches the situation of the MBP data. If one averages over 1000 such $\tilde{\gamma}(q)$, then a constant $\langle \tilde{\gamma}(q) \rangle$ is approached, as illustrated in Fig. 3 for a simulation with $\sigma = 2.55$. However, the distribution of the underlying $\tilde{\gamma}(q)$ becomes wider as q increases.

Unless $q \ll 1$, the form of an individual $\tilde{\gamma}(q)$ tends to be dominated by a small number of very large jumps. If these large jumps occur early in the individual runs, then the resulting $\tilde{\gamma}(q)$ decreases with increasing q ; if they occur late, then $\tilde{\gamma}(q)$ increases with q . For $q \approx 0$, on the other hand, the values of $\tilde{\gamma}(q)$ are not dominated by the few large jumps. They are consistent from one realization to another and characterize the asymptotic mean for all q . We also note that by this mechanism the mean square displacement can present subdiffusive behavior at $q \geq 2$ without explicit inclusion of waiting times between jumps as in the cellular model above.

The spatial scaling of the MBP motions indicates K41 turbulence in the intergranular lanes. The range of the multiscaling is one order of magnitude in scale, but the upper limit is at ~ 1200 km, the granular scale, which should characterize turbulent energy injection. The observed motions are bounded below by instrumental resolution at ~ 100 km. Within 2σ (95%) error bars, as shown in Fig. 5, we find structure function exponents $\zeta_K(q) = q/3$. This is compatible either with K41 hydrodynamic turbulence or with the magnetohydrodynamic turbulence found in the solar wind at 2.8 AU [18]. It is incompatible with the Kraichnan form of magnetohydrodynamic turbulence for which $\zeta(q) = q/4$.

In a broader context, previous experimental work [19] has shown that tracer motion in a rotating flow presents anomalous diffusion which can be analyzed in terms of Lévy flight motions as we have done here. More recent experimental work [20] finds that the separations of particle pairs in a turbulent flow, in the Richardson regime, show a stretched exponential form rather than the Lévy power law form. This result, however, can be recovered from particle pairs undergoing relative motions with an asymmetric Lévy distribution [21].

Our subgranular bright point dynamics exhibit clear temporal multiscaling (Fig. 2). The explicit form of the multiscaling, expressed by the exponent $\gamma(q)$ permits rejection of one model of subdiffusive MBP transport which seems acceptable when examined only in the standard $q = 2$ case. Rather, the observation of such subdiffusion appears to be a matter of chance. More definitively, within the CTRW framework, the diffusion exponent $\gamma(0) \approx 1.3$ shows that the motions instead lie in the superdiffusive intermediate regime between Brownian and Richardson diffusion. This implies that the MBPs are only imperfect tracers of the fluid flows: their motions remain correlated for only finite time (but infinite squared time). This is not surprising in view of the fact

that the MBPs are not truly local objects. Rather, they are the intersections with the photosphere of extended flux tubes which are influenced by various motions. Further, they are restricted to the intergranular lanes.

Finally, in view of the scaling properties of the spatial correlations, as reconciled above with the temporal multiscaling, we suggest that the observed MBP motions are evidence of the expected turbulence in the intergranular lanes of the solar photosphere. Our quantification of the deviation of the MBP motions from the underlying fluid motion should contribute to a better physical understanding of flux tubes and the solar medium.

This work was supported in part by NSF Grants ATM-9628882 and ATM-9987305. The SVST is operated by the Swedish Royal Academy of Sciences at the Spanish Observatorio del Roque de los Muchachos of the Instituto de Astrofísica de Canarias.

-
- [1] R. F. Stein and Å. Nordlund, *Astrophys. J.* **499**, 914 (1998).
 - [2] A. Nesis, A. Hanslmeier, R. Hammer, R. Komm, W. Mattig and J. Staiger, *Astron. Astrophys.* **279**, 599 (1993).
 - [3] T. E. Berger, M. G. Löfdahl, R. A. Shine and A. M. Title, *Astrophys. J.* **506**, 439 (1998).
 - [4] M. G. Löfdahl, T. E. Berger, R. A. Shine and A. M. Title, *Astrophys. J.* **495**, 965 (1998).
 - [5] T. E. Berger, M. G. Löfdahl, R. A. Shine and A. M. Title, *Astrophys. J.* **495**, 973 (1998).
 - [6] T. E. Berger, C. J. Schrijver, R. A. Shine, T. D. Tarbell, A. M. Title and G. Scharmer, *Astrophys. J.* **454**, 531 (1995).
 - [7] T. E. Berger and A. M. Title, *Astrophys. J.* **463**, 797 (1996).
 - [8] R. B. Leighton, *Astrophys. J.* **140**, 249 (1964).
 - [9] J. M. Mosher, Ph. D. Thesis, Calif. Inst. Tech., unpublished (1977).
 - [10] J. Klafter, A. Blumen and M. F. Shlesinger, *Phys. Rev. A* **35**, 3081 (1987).
 - [11] A. C. Cadavid, J. K. Lawrence and A. A. Ruzmaikin, *Astrophys. J.* **521**, 844 (1999).
 - [12] G. W. Simon, A. M. Title and N. O. Weiss, *Astrophys. J.* **442**, 886 (1995).
 - [13] A. N. Kolmogorov, *Dokl. Acad. Nauk. (USSR)* **30**, 301 (1941).
 - [14] U. Frisch *Turbulence: The Legacy of A. N. Kolmogorov* (Cambridge University Press, Cambridge, 1995).
 - [15] H. G. E. Hentschel and I. Procaccia, *Phys. Rev. A* **29**, 1461 (1984).
 - [16] M. F. Shlesinger, B. J. West and J. Klafter, *Phys. Rev. Lett.* **58**, 1100 (1987).
 - [17] G. Zumofen, A. Blumen, J. Klafter and M. F. Shlesinger, *J. Stat. Phys.* **54**, 1519 (1989).
 - [18] W. H. Matthaeus, M. L. Goldstein and C. Smith, *Phys. Rev. Lett.* **48**, 1256 (1982).

- [19] T. H. Solomon, E. R. Weeks and H. L. Swinney, Phys. Rev. Lett. **71**, 3975 (1993).
- [20] M. -C. Jullien, J. Paret and P. Tabeling, Phys. Rev. Lett. **82**, 2872 (1999).
- [21] I. M. Sokolov, J. Klafter and A. Blumen, Phys. Rev. E **61**, 2717 (2000).

FIG. 1. Typical solar MBP trajectory. Distances are in Megameters. Positions were observed at intervals of about 24 s; the total elapsed time is 59 min.

FIG. 2. Moments $\langle r^q \rangle^{1/q}$ of the cumulative solar MBP displacements r in Megameters versus time in minutes for moment orders $q = 1/2, 1, 2, 4$.

FIG. 3. The multiscaling exponent $\gamma(q)$ versus moment order q . Filled circles: solar MBPs, open circles: cellular waiting time model. Open squares: mean of sample distribution generated by CTRW model.

FIG. 4. Longitudinal velocity structure functions of orders 2, 3 versus spatial separation in km.

FIG. 5. Scaling exponents of the structure functions versus order q . Closed circles are from the MBP data with 2σ or 95% error bars. The solid line shows the K41 form.

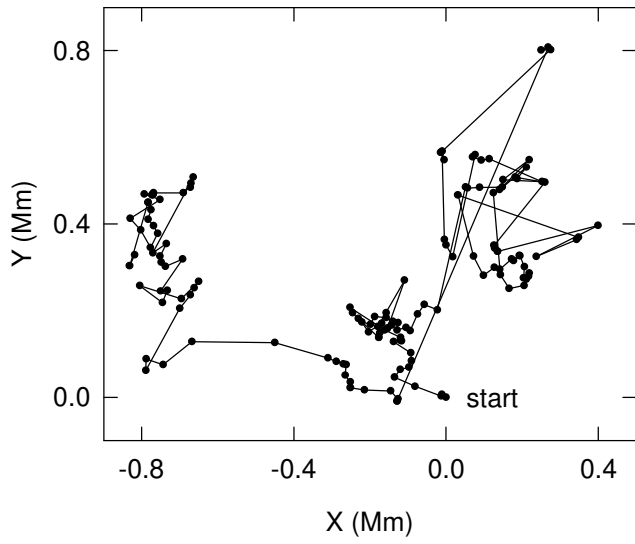


Figure 1

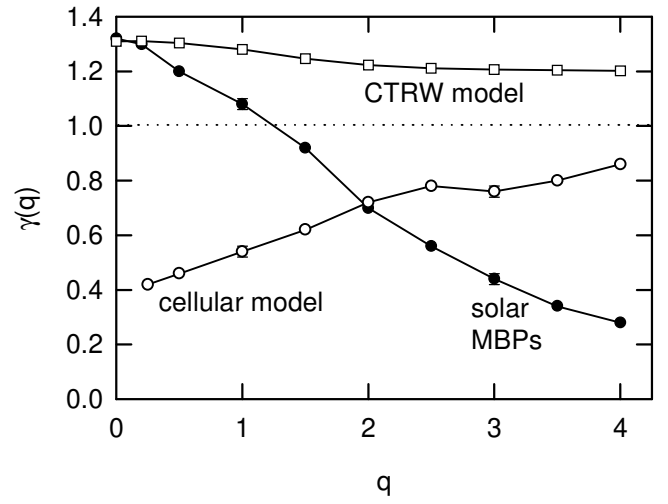


Figure 3

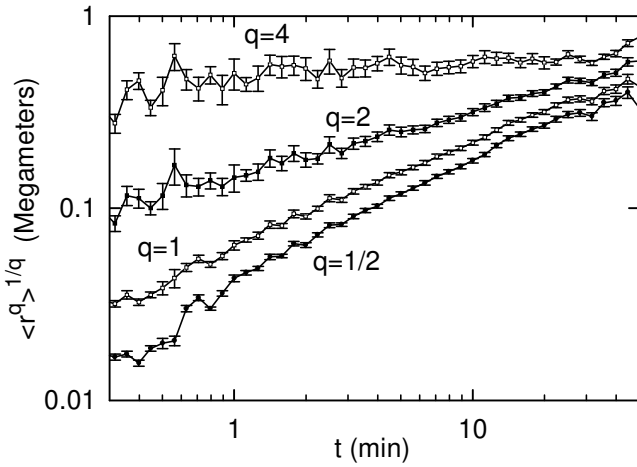


Figure 2

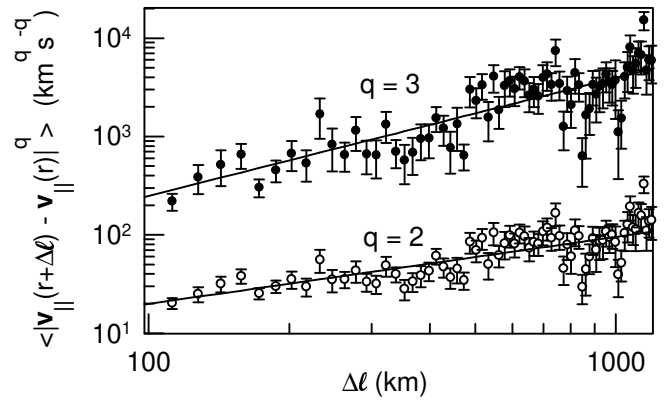


Figure 4

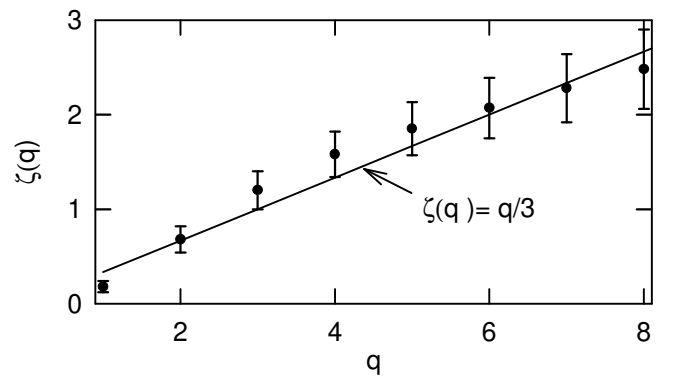


Figure 5

